PREPARED FOR THE U.S. DEPARTMENT OF ENERGY,
UNDER CONTRACT DE-AC02-76CH03073

PPPL-3774
UC-70

PPPL-3774

Wave Driven Fast Ion Loss in the National Spherical Torus Experiment

by

E.D. Fredrickson, C.Z. Cheng, D. Darrow, G. Fu,
N.N. Gorelenkov, G. Kramer, S.S. Medley, J. Menard, L. Roquemore,
D. Stutman, and R.B. White

January 2003

PPPL
PRINCETON PLASMA
PHYSICS LABORATORY

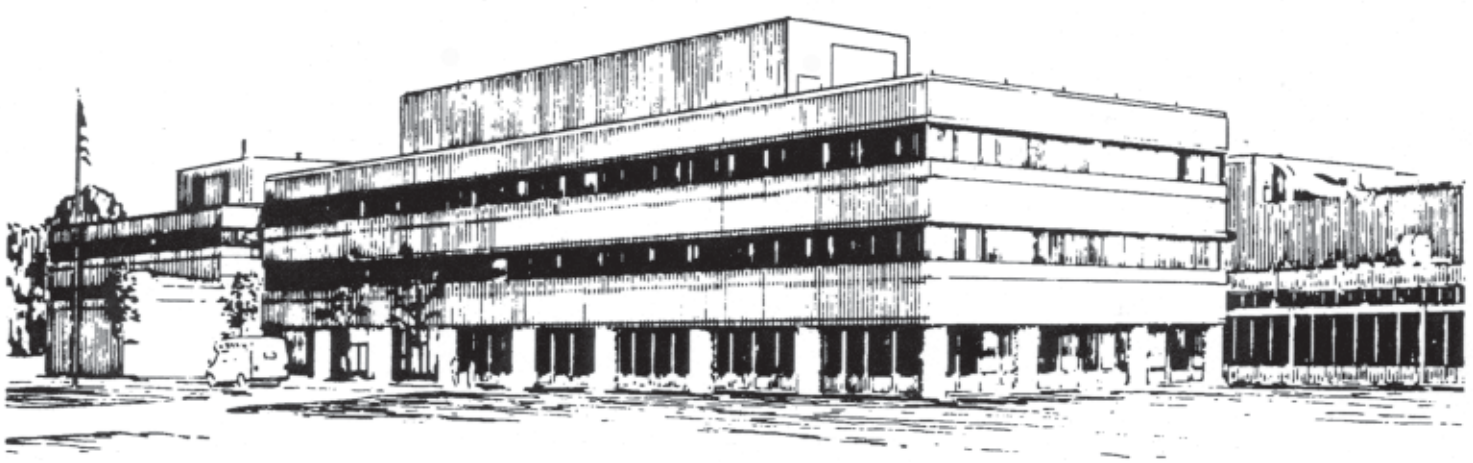

PRINCETON PLASMA PHYSICS LABORATORY
PRINCETON UNIVERSITY, PRINCETON, NEW JERSEY

PPPL Reports Disclaimer

Availability

This report is posted on the U.S. Department of Energy's Princeton Plasma Physics Laboratory Publications and Reports web site in Fiscal Year 2003. The home page for PPPL Reports and Publications is: http://www.pppl.gov/pub_report/

DOE and DOE Contractors can obtain copies of this report from:

U.S. Department of Energy
Office of Scientific and Technical Information
DOE Technical Information Services (DTIS)
P.O. Box 62
Oak Ridge, TN 37831

Telephone: (865) 576-8401

Fax: (865) 576-5728

Email: reports@adonis.osti.gov

This report is available to the general public from:

National Technical Information Service
U.S. Department of Commerce
5285 Port Royal Road
Springfield, VA 22161

Telephone: 1-800-553-6847 or
(703) 605-6000

Fax: (703) 321-8547

Internet: http://www.ntis.gov/ordering.htm

Wave driven fast ion loss in the National Spherical Torus Experiment

E.D. Fredrickson, C.Z. Cheng, D. Darrow, G. Fu,
N.N. Gorelenkov, G Kramer, S S Medley, J. Menard, L Roquemore,
D. Stutman[1], R. B. White

Princeton Plasma Physics Laboratory, Princeton, New Jersey 08543
[1]University of California, Irvine, California 92697

Spherical tokamaks, with their relatively low toroidal field, extend fast ion driven instability physics to parameter ranges not normally accessed in conventional tokamaks. The low field means that both the fast-ion larmor radius normalized to the plasma minor radius and the ratio of the fast ion velocity to the Alfvén speed are relatively large. The large Larmor radius of the ions enhances their interaction with instability modes, influencing the structure of the unstable mode spectrum. The relatively large fast ion velocity allows for a larger population of fast ions to be in resonance with the mode, increasing the drive. It is therefore an important goal of the present proof-of-principle spherical tokamaks to evaluate the role of fast ion driven instabilities in fast ion confinement. This paper presents the first observations of fast ion losses resulting from toroidal Alfvén eigenmodes and a new, fishbone-like, energetic particle mode.

I. INTRODUCTION

Losses of fast ions due to "fishbone" modes [1-4], toroidal Alfvén Eigenmodes (TAE) [5-25] and Energetic Particle Modes (rTAE/EPM) [26-31] have been seen in many conventional aspect ratio tokamaks. In these experiments the fast-ion population is present for the purpose of heating the plasma, and is provided by either neutral beam injection (NBI) or ion cyclotron range of frequency (ICRF) heating. These losses are of concern in that the heating of D-T fusion plasmas is also expected to be primarily by fast ions in the form of the super Alfvénic fusion α's.

In recognition of their potentially deleterious effects on performance in proposed D-T fusion devices, fast ion driven instabilities have been extensively studied in conventional aspect ratio tokamaks. Any substantial loss of the fusion α's would either reduce the ignition margin, or, as importantly, cause damage to plasma facing components. Theoretical modeling of these instabilities and their impact on fast ion confinement, benchmarked against experimental observations, has suggested that the large size and high field of most envisioned fusion reactors will minimize the impact of fast ion driven instabilities. Consistent with this picture, many of the observed fast ion instabilities in the present generation of large, high field tokamaks were relatively benign.

Spherical tokamaks (ST's), including the National Spherical Torus Experiment NSTX [32], are particularly susceptible to fast ion driven instabilities, due primarily to their relatively low toroidal field, but also in some instances due to the direct effect of the low aspect ratio. Indeed, a wide variety of beam driven instabilities has already been seen in NSTX, at frequencies ranging from a few kHz to many MHz[33-36]. The Alfvénic modes are readily excited in NSTX as the neutral beam full energy ion velocity is typically 2-4 times the Alfvén speed and because the Larmor radius of the fast ions is large compared to the minor radius, enhancing mode-particle interactions. The situation in an ST component test facility (CTF) or reactor concept [37] will be very similar, with the fusion α's having similar dimensionless parameters to the beam ions in NSTX.

This paper will focus on two classes of fast ion driven instabilities which have recently been discovered to cause fast ion losses in NSTX. The first of these is the toroidal Alfvén eigenmode (TAE), first seen in conventional aspect ratio tokamaks during Neutral Beam Injection (NBI) and Ion Cyclotron Range of Frequency (ICRF) heated plasmas [5-25]. This instability has been extensively studied over a wide range in parameters in conventional tokamaks and in many cases implicated in enhanced transport of fast ions. The second

instability is different from, but appears related to, the fishbone instability first discovered on the PDX tokamak [1-4] and observed since on most beam heated conventional tokamaks [38-39]. Fishbone-like instabilities with similar characteristics to those seen on NSTX have previously been observed on both DIII-D [40,41] and the Small Tight Aspect Ratio Tokamak, START [42]. Recently a model for the instability, based on a bounce resonance, rather than a precession resonance, has been proposed [43]. The goal of the paper is to present an overview of some of the initial experimental data.

The NSTX is a low aspect ratio ($R/a \approx 1.3$) toroidal device. The plasma major and minor radii are 0.87 m and 0.65 m respectively. The operational parameters for beam heated plasmas are up to 1.5 MA of plasma current, 3 to 6 kG toroidal field at the nominal plasma major radius, central electron density is $0.5 - 8 \times 10^{19}/m^3$, central electron temperature of 0.3 – 1.5 keV. The plasmas were heated with 0.5 to 6 MW of deuterium neutral beam injection power at a voltage of up to 100 kV.

II EXPERIMENTAL RESULTS

An example of a typical spectrum of magnetohydrodynamic (MHD) activity during NBI heating on NSTX is shown in Fig. 1. The frequency range up to 150 kHz includes the resonant toroidal Alfvén eigenmodes (rTAE) or other energetic particle modes (EPM), toroidal Alfvén eigenmodes (TAE), fishbone, and other current and pressure driven MHD modes, but excludes the "compressional" Alfvénic mode (CAE) activity [33-36,44-48]. The higher Alfvén gaps are also not included, but modes in the frequency range of these higher gaps have not yet been observed. The fishbone and TAE modes are often correlated with fast drops in the neutron rate and bursts in the D-alpha emission (Figs. 1b and 1c) on NSTX. These observations are taken to indicate losses of fast ions.

The low toroidal field on NSTX, as well as the relatively high rotation rates, result in a spectrum that is not as well separated as is the case in large, high field conventional aspect ratio tokamaks, where the TAE gaps are typically an order of magnitude higher in frequency than the typical MHD frequencies. On NSTX central rotation rates can be up to 20 – 30 kHz, while near the edge the rotation is typically 2 – 5 kHz. Thus, an n=2 mode with zero frequency in the plasma frame can have a frequency in the lab frame from a few kHz to over 50 kHz. The higher end of this range, corresponding to a mode in the core, is comparable to the first, off-axis TAE gap frequency's. The initial, high frequency, phase of the fishbone instabilities, which correspond to the fast ion bounce or precession frequencies, also

commonly begin near the TAE gap range of frequencies. This overlap of lab-frame frequency ranges makes identification of modes, based on frequency alone, problematic.

TAE modes are a natural, weakly damped resonant oscillation of the plasma. The frequency of TAE modes is determined by plasma parameters such as the Alfvén velocity (a function of density and magnetic field strength) and magnetic field geometry through the TAE-gap structure. For TAE modes localized outside the q=1 surface (to exclude fast profile changes due to sawteeth), the mode frequencies should change only slowly with time, *i.e.*, on current diffusion or density confinement timescales. Thus modes with frequencies in the first TAE gap frequency range and whose frequency changes slowly have been tentatively identified as TAE modes. The TAE can have either a strongly bursting character, i.e., the mode periodically grows quickly, then disappears, or reach a quasi-saturated state where the mode amplitude evolves on equilibrium evolution timescales. This difference in behavior has been studied in the context of TAEs in conventional aspect ratio tokamaks and can be modeled by a predator-prey type relationship [16]. Theoretical modeling of these modes using the best available measurements of plasma equilibria have begun.

In this same frequency range, modes which rapidly "chirp" (sweep downward) in frequency have also been seen. As changes in mode frequency on this timescale are very unlikely to represent changes in equilibrium plasma conditions, these modes are believed to be of the generic class of Energetic Particle Modes (EPM). For these modes, the frequency is determined by the resonance condition with the fast ion distribution, with the fastest mode growth rate at the frequency that maximizes the energy transfer rate from the fast ions to the mode. As the mode grows and modifies the fast ion distribution, the mode frequency evolves to keep the drive at a maximum. The strong chirping of these particular modes on NSTX is suggestive of the fishbone instability discovered on PDX. While these modes are clearly not exactly the same, we refer to them here generically as fishbones. These modes will be discussed in more detail in Sect. IIb.

IIa TAE-induced fast ion loss

For most NSTX beam heated plasmas, TAE modes, when present, are quasi-continuous and have no detectable effect on plasma performance. However, in experiments in which H-modes, with broad density profiles, were created in plasmas with relatively high q on axis (deduced with EFIT [49,50]) the TAE modes became strongly bursting. Concurrently with

the bursts, fast drops in the neutron rate were observed as well as bursts of fast-ion losses and D-alpha bursts. These observations suggest substantial losses of fast beam ions.

An example of such a shot is shown in Fig. 2. Figure 2a shows the time evolution of the neutral beam heating power and the plasma current for a 650 kA shot. Shortly after the beam power is stepped up to 3.2 MW, the plasma goes into H-mode (evidenced by the drop in D-alpha light at 0.232s in Fig. 2b). Spikes in the D-alpha light are seen during the H-mode phase, coincident with drops in the neutron rate (Fig. 2c). These spikes are not ELMs, since there is no drop in edge soft x-ray emission which occurs with ELMs. These events are correlated with strong bursts of coherent MHD activity (Fig. 2d). (The neutron diagnostic timing is uncertain to ≈1 ms, precluding a more detailed correlation of the timing of the neutron drop with mode growth.)

The drop in the neutron rate is ≈ 10 – 15% for each burst. The neutron production, S, is mostly from beam-target reactions (≈ 75% beam-target, ≈ 25% beam-beam and < 0.1% thermal). Assuming that the lost ions are the most energetic, this drop corresponds to a similar drop in the population of the most energetic ions (the neutron production is a very steep function of the fast ion energy). The drop in fast ion density is slightly less than linear in the drop in neutron rate (because of the contribution of the beam-beam neutrons), and for small perturbations in these plasmas $\delta n_{fast} / n_{fast} \approx 0.8\ \delta S / S$. Estimating the fast ion slowing down time to be $\tau_{slow} \approx 55$ ms, the average period between bursts to be about $\tau_{burst} \approx$ 6 ms and the average neutron rate drop to be $\delta S \approx 12\%$, or the drop in $n_{fast}\ \delta n_{fast} \approx 10\%$, it can be roughly estimated that the effect, in equilibrium, of such modes would be to drop the fast ion population by approximately 50% [13,51]. (This assumes a constant source and the dominant fast ion energy loss mechanism, excepting the TAE bursts, to be classical slowing down.) In practice, of course, if the instabilities can cause substantial losses, they will keep the fast ion beta near the threshold for excitation.

Bursts of D-alpha light correlated with each TAE burst and neutron drop are evidence that the fast ions expelled from the plasma are striking the divertor plates. The loss of fast ions has also been independently confirmed by direct measurement of ion losses with a fast-ion loss probe [52]. The probe is mounted on the outboard vacuum vessel midplane. The present detectors do not resolve pitch angle or energy, but do detect bursts of loss coinciding with each TAE burst.

In Figure 2d is a graph of the time evolution of the rms magnetic fluctuation level integrated over the frequency range from 80 to 150 kHz. The modes have a roughly exponential growth in the time period between the bursts. The approximate average growth rate, as indicated for a couple of bursts, is about 500 s^{-1}, or $\gamma/\omega \approx 1.6 \times 10^{-3}$. There is significant variation in this estimated growth rate, and the final growth rate at the end of each period does appear to be significantly larger, with $\gamma/\omega \approx 6 \times 10^{-3}$. The peak rms TAE mode amplitude has reached nearly 1 G when the neutron drop occurs.

The effect of fast ion losses on other fast ion driven modes is also of interest. The rms magnetic fluctuation levels in two other frequency bands; 10 – 40 kHz corresponding to the fishbone modes discussed below, and 500 – 1500 kHz corresponding to the CAE frequency band are shown in Fig. 2e and 2f, respectively. Three strong fishbone bursts are seen in this time period, indicated by the bold vertical lines in the figure. Interestingly, there is no apparent effect on the TAE amplitude for the first two bursts, and none of the fishbone bursts is correlated with particularly large drops in the neutron rate. However, the drop in the CAE amplitude following each fishbone is evidence that the fishbones modify the fast ion population (Fig. 2f). There is no similar effect of the TAE bursts on the CAE, despite the drops in neutron emission correlated with the TAE bursts. These observations suggest that the TAE are excited by, and cause loss of, a different population of fast ions from those which drive the CAE, separated either in physical or phase space. The fishbones, however, interact with populations driving both CAE and TAE. These observations are consistent, for example, with a model that the CAE are localized far off-axis and the TAE are primarily driven by, and cause the loss of, core fast ions.

In Fig 3 is shown a spectrogram of the Mirnov data shown in Fig. 2c. The frequency of the modes in the MHD bursts is seen to be roughly in the range from 80 – 130 kHz. The toroidal mode numbers of each of the bursts are indicated by colors as described in the figure caption. The mode numbers are calculated from Fourier transform phases on ≈ 0.5 ms intervals using a toroidal array of 12 Mirnov coils. Also shown is the time evolution of the estimated core TAE frequency, $V_{Alfvén}(0)/4\pi qR$, together with the approximate Doppler shifted frequencies for the dominant toroidal mode numbers n = 2 and n = 3. Modes with toroidal mode numbers ranging from n=2 up to n=5 are present. The spacing of the dominant TAEs is roughly consistent with the spacing expected from the Doppler shift.

Each final burst is seen to consist of several modes with toroidal mode numbers ranging from n=2 to n=6. This is shown more clearly for the burst at 0.283 s in Fig. 4. The spectrum

of the time derivative of the magnetic fluctuation contains at least six modes. The mode numbers of the primary spectral components are indicated in the figure. Note that at least two peaks share the same mode number, n=4. The shortness of the burst precludes better spectral resolution, and there could be additional unresolved modes in the large peaks. The presence of multiple modes may also enhance the fast ion transport [53].

Figure 5 shows the gap structure for the n=2 mode, calculated with NOVA [54] based on the measured density profile and the q profile inferred from EFIT. The gap becomes quite narrow near the axis as q(0) approaches 2. There is considerable uncertainty in the q profile; even as little as a 10% change in q(0) will open the gap. Nevertheless, the gap structure is probably qualitatively correct, showing a quite wide gap away from the axis. Improved resolution will have to wait for new diagnostics.

IIb "Fishbone" induced losses

Chirping modes are seen in NSTX with frequencies beginning at over 100 kHz and chirping down to a few kHz on a timescale of milliseconds. The timescale for the chirping, together with the short repetition time, suggests that these are fast ion driven instabilities which are affecting the beam fast ion distribution. The bursting and chirping are qualitatively similar to the behavior of the fishbone mode seen in conventional-aspect ratio tokamaks. However, the frequency range of the chirps can be much larger than for conventional fishbone modes and the toroidal mode number is not necessarily unity, but can be as large as n = 5.

The chirping modes on NSTX can be qualitatively separated into two groups. The first group, herein referred to as Type II (classic fishbones would be Type I), consists of modes with frequency characteristics similar to those of the original fishbone mode. However, the frequency chirp starts near the upper range of fast ion bounce, rather than precession, frequencies and approaches zero in the plasma frame at the low frequency end. The downward chirp can be accompanied by fast ion losses, inferred from a transient drop in the neutron rate, directly measured increases in fast ion losses and bursts of D-alpha as the fast ions hit the plasma facing components. On NSTX, the repetition rate for this type of mode can range from essentially isolated events to periods as short as 5 – 10 ms. Unlike the original fishbone instability, this mode often occurs when the inferred q(0) is well above unity. Further, the mode is not limited to a toroidal mode number of n=1, but ranges up to at least n=5.

The second group of fishbone-type modes (referred to as Type III) tends to have higher frequencies, is generally n=1, and has a smaller frequency range in the chirps. They are also much more common, occurring in virtually every NSTX NBI heated plasma. They begin shortly after the start of NBI heating during the current ramp and end, typically, about the time the current flattop starts. As yet, there has been no detected impact of these modes on fast ion confinement. As these modes overlap the first toroidal Alfvén eigenmode gap, they may also be a form of resonant toroidal Alfvén Eigenmode (rTAE) or energetic particle mode (EPM).

Most of the features of the fishbone-type modes described above can be seen in the spectrogram shown in Fig. 6. Here the fitted toroidal mode numbers are again indicated by colored contours. The Type III fishbones are the black band between 0.1 and 0.2 s and roughly between 50 and 90 kHz. The individual bursts of these modes are so close together that they are not resolved.

The Type II fishbones bursts occur less frequently and often evolve throughout the shot with the toroidal mode increasing from n=1 up to n=5. The first Type II fishbone occurs between roughly 0.14 and 0.15 s. During this approximately 10 ms interval, the mode frequency drops from about 25 kHz to about 5 kHz. The mode number is n=1. The q(0) is inferred by an EFIT equilibrium calculation to be approximately 1.8. Three or four fishbones with n=2 (red) then follow during the period from 0.18 s to 0.21 s. This sequence continues as the toroidal mode numbers increase through n=3 (green), n=4 (blue) and n=5 (yellow).

Below the spectrogram is shown the time evolution of the neutron flux. The first type II fishbone results in a discernable pause in the rise of the neutron rate. Only this fishbone, and the fishbones at 0.205 s and 0.265 s cause a relatively small, drop in the neutron rate. Thus, many of these type II fishbones also had little impact on the neutron rate.

While the edge magnetic fluctuation level is at best an indirect measure of the internal mode amplitude, there is also a correlation between the impact on the neutron rate and the edge magnetic fluctuation amplitude. In Fig. 7 is shown the rms magnetic fluctuation level and again the time evolution of the neutron rate. Clearly the two largest modes, as measured by Mirnov coils on the outboard midplane are those which result in two of the three significant neutron rate dips. This suggests that those fishbones which had the strongest effect were also those that swept to the lowest frequencies. While there is some agreement between the low end of the fishbone chirp and the bulk plasma rotation frequency, it is

clearly not exact. As there is substantial shear in the plasma rotation, accurate modeling of the expected mode frequencies will present something of a challenge.

During the sequential evolution of the toroidal mode number from n=1 up to n=5 the current profile continues to peak, with q(0) decreasing from somewhere near $q(0) \approx 2$ at the time of the n=1 fishbone, to $q(0) \approx 1$ by the time of the n=5 fishbones. During this time, the plasma density increases from 2×10^{19} /m^3 to 3×10^{19} / m^3, which may affect the fast ion distribution. Thus it is also possible that the mode number evolution reflects an evolution in the fast ion distribution.

Some indication of the internal structure of the fishbone modes is also visible in the soft x-ray data. In Figure 8 are shown the soft x-ray traces from a pinhole camera [55] observing the plasma in the nominal horizontal direction. In Fig. 8a, the individual traces are auto-scaled and graphed at their approximate tangency (midplane minor) radius through the time period of the fishbone which results in the first large drop in neutron emission. There is an inversion in the oscillations between 0.2 m and 0.25 m in minor radius. This inversion could be either due to the presence of an island at this location or an effect of the chord integration. The much weaker Type III fishbones can also be seen in this figure before and after the Type II fishbone. The bandwidth of the soft x-ray camera is > 100 kHz, so the higher frequency modes are not suffering from attenuation. However, if the poloidal wavelength of the Type III fishbones was much shorter than the Type II, the chord integration could reduce the apparent amplitude.

Interpretation of soft x-ray data is difficult due to the complicated dependence on plasma parameters and the chord integration. Figure 8b shows the chord integrated soft x-ray profile. There is a strong gradient in the chord integrated emissivity profile between roughly r = 0.15 m and r = 0.45 m. Within this range the soft x-ray data will be more sensitive to displacements than in regions where the emissivity profile is flatter.

For comparison, Figure 9, (in the same format as Figure 8), shows the n=2 fishbone at 0.195 s. In this case the mode amplitude in the soft x-ray signal appears much weaker than for the example in Fig. 8, while the amplitude on the Mirnov coil is only slightly smaller, suggesting that the radial structure of the mode is different. The fluctuations from the fishbone are circled in red. The radial location of the mode appears similar; however, as the soft x-ray emissivity drops precipitously towards the plasma periphery, it is not clear that there is sufficient sensitivity in the edge channels to conclude that the mode amplitude is weaker here.

The fishbone event at 0.205 s is more complex. The fishbone appears to be triggered by a small sawtooth-like event. In this case it is possible that some of the fast ion losses are due directly to the sawtooth event. The soft x-ray emissivity is flat or hollow in the core region, precluding detailed reconstruction of the event, however the sawtooth event has a lower frequency precursor. In Fig. 10 are shown the soft x-ray traces from the lower camera up to the onset of the fishbone mode. A low frequency mode at 7 kHz (and n=1 on the Mirnov array) is growing until ≈ 0.2054 s. During the final growth, an increase in the soft x-ray emissivity is seen on the soft x-ray chords between ≈ 20 and ≈ 40 cm. Soft x-ray emissivity profiles from before and after this event are shown in Fig. 10b. The emissivities are inferred by inverting the chord integrated data as constrained by the EFIT equilibria. The inversions suggest that the emissivity drops in the core region and increases outside a minor radius of about 0.28 m, i.e., consistent with a sawtooth-like event. EFIT, however, calculates $q(0) \approx 1.3$ at this time and the event is much weaker than the sawteeth normally seen on NSTX.

In Fig. 11 is shown a spectrogram of a 0.8 MA shot with 6 MW (at 90 kV) of neutral beam heating power. Again, fishbones, with a somewhat longer period, are causing 20% transient drops in the neutron rate. In this case the later fishbones between 0.24 and 0.29 s have a toroidal mode number of n=3 whereas the earlier fishbones are a combination of n=2 and n=1 modes. The earlier fishbones, while reaching similar fluctuation amplitudes on Mirnov coils and soft x-rays, had a much smaller effect on the neutron rate. That could mean either that the structure of the n=3 mode interacted more effectively with the fast ion distribution or that the n=2 modes interacted primarily with lower energy fast ions whose loss didn't as seriously impact the neutron rate. More detailed studies with improved diagnostics, coupled with advanced theoretical models will be required to sort these issues out.

In Fig. 11c is shown the D-alpha emission from the upper divertor region. The drop in D-alpha at 0.26 s indicates an H-mode transition. In this shot, and many others, there is a fishbone at or just preceding the H-mode transition, suggesting that fishbones could help to trigger an H-mode (e.g., by expelling fast ions which charges the plasma up and induces rotation [56]). This conjecture is bolstered by the observations that the two fishbones preceding the H-mode transition result in D-alpha drops, suggestive of dithering H-modes. The fishbone following the H-mode transition is correlated with a small spike in D-alpha, as in the bursting TAE examples. However, fishbone bursts are not as clearly correlated with D-alpha bursts, even fishbone bursts with large neutron drops. This may indicate that the fast ions are lost to a different, unobserved, part of the machine.

IIc Induced losses in the presence of multiple modes.

TAE modes often co-exist with fishbone modes, and under some circumstances the TAE bursts also appear to trigger fishbones. In Fig. 12a is shown a spectrogram of a shot in which many of the fishbones are apparently triggered by TAE bursts. Below the spectrogram is shown the neutron evolution (Fig. 12b) and in Fig. 12c the envelope of the magnetic fluctuation level for the frequency bands 5 – 50 kHz (fishbones) and 70 – 110 kHz (TAE). The drop in the neutron rate is as large as 20% for the later bursts, and the repetition period is approximately 10 ms, or roughly one third of the fast ion slowing down time. The effect of periodic losses of fast ions can be simply estimated, based on the assumption of short periodic bursts of losses, a constant replenishment rate and exponential slowing down time for the fast ions. For the roughly 10 ms period of 15% losses, the effect on the "steady state" fast ion population suggests that in steady-state, such modes would reduce the fast ion population by ≈ 40%.

In the latter phase of long pulse, high beta discharges, the fishbones often have multiple toroidal mode numbers (n=1 through n=3 or 4). The fast ion losses from these events can be substantial; neutron drops as large as 25% have been seen (Fig. 13). For these fishbones, large bursts in the Neutral Particle Analyzer (NPA) [57,58] signal have been observed coincident with the fishbone chirps on the Mirnov data. An example, from the latter half of the discharge shown in Fig. 12, is shown in Fig. 13. Such bursts have been observed over a wide range in the NPA tangency radii of R_{tan} = 15 - 92 cm.

The fishbone-induced bursts are observed at all energies in the neutral beam ion spectrum "chirp" (sweep downward) in energy as illustrated in Fig. 14. Shown are the energetic ion spectra with 1 ms time resolution for 1 ms before the fishbone (black curve), the first (red curve) and second (blue curve) millisecond of the fishbone chirp and 1 ms after the end of the fishbone (purple curve). During the first millisecond of the fishbone, the entire energy spectrum increases by approximately two e-foldings or a factor of 5 – 10. During the following millisecond, the spectrum above ~ $E_b/2$ approaches the pre-fishbone level (*i.e.,* the ion loss terminates) while ions below $E_b/2$ continue to be elevated (ion loss continues). In the millisecond after the fishbone, the spectrum above $E_b/2$ is depleted by ~ 25 % relative to the pre-fishbone level, a loss in energetic ion population that is consistent with the observed drop in the neutron yield.

With occasional exceptions, bursts in the NPA signal due to fishbones are not correlated with spikes in the D-alpha emission nor with features in the ion loss signal from the iFLIP lost ion diagnostic. In conjunction with observation of fishbone-induced enhancement of the NPA signal at all energies, this argues that the fishbones cause redistribution of a fraction of the NB ion distribution from the plasma core to more peripheral regions where the higher background neutral signal leads to the observed burst in the NPA signal. To date, no effect has been observed on the thermal deuterium ion spectra due to fishbone activity.

III Discussion

The estimated impact on fast ion confinement of the strongly bursting TAE modes, the fishbone-like instability, or a combination of these two modes can be quite significant. For the most extreme examples, the fishbone bursts, in steady state, would reduce the fast ion population by 50% (c.f., Fig. 11 with 20% neutron drops every 10 ms). Since fast ion loss will directly impact the ignition margin in reactors, it is important to understand the scaling of the loss. Just as important as the impact on ignition margin is the impact of the fast ions on the reactor first wall. In reactors, the fast ion population is measured in 100's of MJ, thus it is also important to determine how localized in time and space the power deposition is from the fast ion loss.

The observation of bursting TAE causing fast ion losses is not new. The first observations of TAE modes in a conventional aspect ratio plasma were accompanied by fast ion losses similar in magnitude to those observed here [2]. However, reactor versions of conventional aspect ratio tokamaks are high field (5 – 10 T), high current (up to 20 MA) with large minor radius (several meters). In this regime, the TAE activity was predicted, at worst, to affect the fast ion population diffusively. This is not so clearly the case for a reactor concept like ARIES-ST [37]. The normalized alpha larmor radius is somewhat smaller than on NSTX (0.04 compared to 0.2), but not much smaller than that of conventional tokamaks (0.06 - 0.09) where substantial TAE induced losses were seen[6,59]. Further, the parameter regime where the bursting TAE modes are observed in NSTX, i.e., with broad density (pressure) profile and elevated q on axis, is the regime proposed for long pulse, high bootstrap fraction ST operation.

The "fishbones" have been identified as a type of "energetic particle mode" (EPM), based largely on the strong frequency chirping. Energetic particle modes are strongly driven instabilities whose frequency is determined by the optimized resonance condition with the

fast ion distribution. Because the mode frequency is not set by equilibrium plasma properties (such as density or magnetic field strength), the frequency can change as quickly as the mode can modify the fast ion distribution. The original fishbone model, developed to fit the observations made on PDX, was a resonance of the mode with the precession-drift of the fast ions [1-4]. The peak in the energy transfer (from fast ions to mode) occurred at the highest frequency with the most energetic ions. As the most energetic ions were lost, the optimum resonance frequency dropped, coupling to lower energy ions. Thus, a characteristic of the fishbones was a strong downward chirp in frequency. The bursting character followed the classic predator-prey relation[16]. Although the fishbones on NSTX have significant differences from classic fishbones, they retain two features of the classic fishbones, namely the strong chirping and the bursting character.

The classic fishbone (Type I) was a predominantly m=1, n=1 instability in plasmas with $q(0) < 1$. In NSTX the fishbones have been seen with toroidal mode numbers from n=1 to n=5. They are also most commonly seen in plasmas with q(0) well above unity, implying m>1. Because of the high beta and low aspect ratio the precession frequency in an ST can be quite small, and in some cases reverses direction. Thus, it is believed that the resonance drive in NSTX is through the fast ion bounce resonance [34]. For this resonance condition to be strong, the average bounce angle (angle of banana turning points) must be large. For many beam heated shots on NSTX there is a large population of fast ions, not necessarily the most energetic, which have large bounce angles. A similar situation is expected in fusion-alpha heated reactors where the alpha population is intrinsically isotropic. This resonance condition should still retain the feature that the energy transfer rate is proportional to the mode frequency; the modes should still appear first with high frequency, and chirp down as the fast ions are lost.

The discovery of these bounce-resonance fishbones on NSTX is significant in that the classic fishbones were predicted to be stable in conventional aspect ratio fusion reactors (and NSTX) as the high beta resulted in small precession frequencies (i.e., weak drive). The proposed bounce-resonance drive model requires further comparison to NSTX results before it can be applied to reactor-relevant conditions. The observation of bursting TAE modes correlated with fast ion losses also underscores the importance of extending TAE physics models to the ST regime.

Summary

Clear evidence of fast ion losses has been seen in conjunction with at least two forms of fast ion driven instabilities in the spherical torus NSTX. In H-mode plasmas with elevated q on axis, bursting TAE modes causing 10-15% neutron drops were seen. From the burst frequency and estimated slowing down time, these modes in steady state would result in an average 40% reduction of the fast ion population. This regime is similar to that envisioned for a bootstrap-current-driven ST reactor. The dimensionless parameters of the alpha particles are similar to those of the neutral beam ions in NSTX, although the beam ion distribution also includes substantial half and third energy components, and is less isotropic than the fusion alpha distribution is expected to be. Further theoretical modeling is required to evaluate the importance of TAE modes in ST reactors.

Bursting, chirping modes were also seen to cause fast ion losses at rates up to 20% fast ion loss per burst. This would correspond to as much as a 50% reduction in fast ion population in steady-state. These modes differ substantially from the normal fishbone modes seen in conventional aspect ratio tokamaks. Toroidal mode numbers for these modes have been seen between n=1 and n=5. They are typically seen when the q(0) is believed to be well above unity. Finally, the modes are often present when the beam-ion precession frequency is nearly zero – a condition generally assumed to be stable to fishbones. A theoretical model for these modes has been separately proposed [34].

Acknowledgements

We are grateful to the NSTX team for supporting these experiments. We also wish to acknowledge very useful discussions with Drs. G Fu and S Jardin and thank them for their contributions to this work. The help of Drs. M G Bell and S Kaye in the preparation of this manuscript are also greatly appreciated. This work supported by U.S. DOE Contract DE-AC02-76CH03073.

Bibliography

[1] K. M. McGuire, R. Goldston, M Bell, et al., Phys. Rev. Lett. **50** 891 (1983).

[2] R B White, R J Goldston, K M McGuire, et al, Phys. Fluids **26** (1983) 2958.

[3] L Chen, R B White, M N Rosenbluth, Phys. Rev. Lett. **52** 1122 (1984)

[4] W W Heidbrink, K Bol, D Buchenauer, R Fonck, G Gammel, K Ida, R Kaita, S Kaye, H Kugel, B LeBlanc, W Morris, M Okabayashi, E Powell, S Sesnic, and H Takahashi, Phys. Rev. Lett. **57** 835 (1986).

[5] C.Z. Cheng and M.S. Chance, Phys. Fluids **29**, (1986) 2471.

[6] K.L. Wong, R.J. Fonk, S.F. Paul, et al., Phys. Rev. Lett. **66**, (1991) 1874.

[7] J R Wilson, K L Wong, E D Fredrickson, Z Chang, R Nazikian, E Mazzucato, D Darrow, C K Phillips, G Y Fu, M P Petrov, A V Khudaleev, *Proc. 14th Int. Conf. On Plasma Physics and Controlled Nuclear Fusion Research* (Vienna: IAEA) Vol. I, p661 (1992).

[8] K L Wong, Plasma Phys. and Control. Fusion **41** PR1 (1999).

[9] D S Darrow, S J Zweben, Z Chang, C Z Cheng, M D Diesso, E D Fredrickson, E Mazzucato, R Nazikian, C K Phillips, S Popovichev, M H Redi, R B White, J R Wilson, K L Wong, Nucl. Fusion **37** 939 (1997).

[10] S J Zweben, R V Budny, D S Darrow, S S Medley, R Nazikian, B C Stratton, E J Synakowski, G Taylor, Nucl Fusion **40** p91 (2000).

[11] R.B. White, E.Fredrickson, D. Darrow, M. Zarnstorff, R. Wilson, S. Zweben, K. Hill, Y. Chen, and G. Fu, Phys. Plasmas **2** (1995) 2871.

[12] W W Heidbrink, E J Strait, E Doyle, G Sager, R T Snider, Nucl. Fusion **31** (1991) 1635.

[13] H H Duong, W W Heidbrink, E J Strait, T W Petrie, R Lee, R A Moyer, J G Watkins, Nucl. Fusion **33**, 749 (1993).

[14] H.H. Duong, W.W Heidbrink, Nucl. Fusion **33** 211 (1993).

[15] E J Strait, W W Heidbrink A D Turnbull, M S Chu, H H Duong, Nucl. Fusion **33** 1849 (1993)

[16] W W Heidbrink, H H Duong, J Manson, E Wilfrid, C Oberman, Phys. Fluids **B 5** 2176 (1993).

[17] M Saigusa, h Kimura, S Moriyama, Y Neyatani, T Fujii, Y Koide, T kondoh, M Sato, M Nemoto, Y Kamada, and JT-60 team, Plasma Phys. Control. Fusion **37** 295 (1995).

[18] H Kimura, M Saigusa, S Moriyama, T Kondoh, Y Neyatani, T Ozeki, T Nishitani, Y Kusama, T Fujii, M Sato, M Nemoto, K Tobita, C Z Cheng, Phys. Lett. A **199**, 86 (1995).

[19] M Saigusa, H Kimura, Y Kusama, G J Kramer, T Ozeki, S Moriyama, T Oikawa, Y Neyetani, and T Kondoh, Plasma Phys. Control. Fusion **40** 1647 (1998).

[20] G. Kremer, et al., Nucl. Fusion **40** (2000) 1383.

[21] K. Tobita, et al., Fusion Science and Tech. **42** (2002) 315.

[22] S Ali-Arshad and D J Campbell, Plasma Phys. and Control. Fusion **37** 715 (1995).

[23] A Fasoli, D Borba, G Bosia, D J Campbell, J A Dobbing, C Gormezano, J Jacquinot, P Lavanchy, J B Lister, p Marmillod, J M Moret, A Santagiustina, and S Sharapov, Phys. Rev. Lett. **75** 645 (1995).

[24] A Fasoli, D Borba, C Gormezano, R Heeter, A Jaun, J Jacquinot, W Kerner, Q King, J B Lister, S Sharapov, D Start, and L Villard, Plasma Phys. and Control. Fusion **39** B 287 (1997)

[25] A Fasoli, J A Dobbing, C Gormezano, J Jacquinot, J B Lister, S E Sharapov, A Sibley, Nucl. Fusion **36** 258 (1996).

[26] C Z Cheng, N N Gorelenkov, and C T Hsu, Nucl. Fusion **35**, 1639 (1995).

[27] F Zonca and L Chen, Phys. Plasmas **3**, 323 (1996).

[28] E.D. Fredrickson, M G Bell, R Budny, Z Chang, C Z Cheng, G Y Fu, E Mazzucato, R Nazikian, A T Janos, K. M. McGuire, R Majeski, C K Phillips, G Schilling, G Taylor, and J R Wilson, Nuclear Fusion **35** (1995) 1457

[29] S. Bernabei, M G Bell, R V Budny, E D Fredrickson, N N Gorelenkov, J C Hosea, R Majeski, E Mazzucato, C K Phillips, G Schilling, and J R Wilson, Phys. Rev. Lett. **84**, 1212 (2000).

[30] S Bernabei, R V Budny, E D Fredrickson, et al., Nucl. Fusion **41** (2001) 513.

[31] S. Bernabei, M.G. Bell, R. Budny, D. Darrow, E.D. Fredrickson, N. Gorelenkov, J.C. Hosea, R. Majeski, E. Mazzucato, R. Nazikian, C.K.

Phillips, J.H. Rogers, G. Schilling, R. White, J.R. Wilson, F. Zonca, and S. Zweben, Physics of Plasmas **6**, 1880 (1999).

[32] M. Ono, S M Kaye, Y-K M Peng, *et al*., Nucl. Fusion **40** (2000) 557.

[33] E.D. Fredrickson, N. Gorelenkov, C.Z. Cheng, R. Bell, D. Darrow, D. Johnson, S. Kaye, B LeBlanc, J Menard, S Kubota, W Peebles, Proc.of 28th EPS Conf. on Controlled Fusion and Plasma Physics, Funchal, 2001, ECA vol. 25A (2001), p. 1001.

[34] E D Fredrickson, C Z Cheng, L Chen, D Darrow, N N Gorelenkov, D Johnson, S Kaye, S Kubota, J Menard, R B White, Proc.of 29th EPS Conf. on Controlled Fusion and Plasma Physics, Montreau, 2002, paper P-1.104.

[35] E.D. Fredrickson, N. Gorelenkov, C.Z. Cheng, R. Bell, D. Darrow, D. Johnson, S. Kaye, B. LeBlanc, J. Menard, S. Kubota, W. Peebles, Phys. Rev. Lett. **87**, (2001) 145001.

[36] E D Fredrickson, N N Gorelenkov, C Z Cheng, R. Bell, D. Darrow, D. Gates, D. Johnson, S. Kaye, B. LeBlanc, D. McCune, J. Menard, S. Kubota, W. Peebles, Phys. of Plasmas **9** (2002) 2069.

[37] S C Jardin, C E Kessel, J Menard, T K Mau, R Miller, F Najmabadi, V Chan, L Lao, Y R linliu, R L Miller, T Petrie, P Politzer, A D Turnbull, *accepted for publication* Fusion Engineering and Design,

[38] R Kaita, R B White, A W Morris, E D Fredrickson, K M McGuire, S S Medley, T J Murphy, and S D Scott, Phys. Fluids B **2** 1584 (1990).

[39] M F F Nave, D J Campbell, E Joffrin, F B Marcus, G Sadler, P Smeulders, K Thomsen, Nucl. Fusion **31** (1991) 697.

[40] W W Heidbrink, Plasma Physics and Controlled Fusion **37** (1995) 937.

[41] W W Heidbrink, E M Carolipio, R A James, E J Strait, Nucl. Fusion **35** (1995) 1481.

[42] K G McClements, M P Gryaznevich, S E Sharapov, R J Akers, L C Appel, G F Counsel, C M Roach, R Majeski, Plasma Phys. Contol. Fusion **41** (1999) 661.

[43] E D Fredrickson, L Chen, R B White, *submitted to* Physics of Plasmas.

[44] S.M. Mahajan , D.W. Ross, Phys. Fluids **26** (1983) 2561.

[45] B. Coppi, S. Cowley, R. Kulsrud, P. Detragiache, and F. Pegoraro, Phys. Fluids **29**, (1986) 4060.

[46] N.N. Gorelenkov, C.Z. Cheng, Nucl. Fusion **35**, (1995) 1743.

[47] N N Gorelenkov, C Z Cheng, E Fredrickson, E Belova, D Gates, S Kaye, G J Kramer, R Nazikian, R B White, Nucl. Fusion **42** (2002) 977.

[48] N N Gorelenkov, E Fredrickson, E Belova, C Z Cheng, D Gates, S Kaye, R B White, in *19th IAEA Fusion Energy Conference, Lyon, France, 14-19 Oct 2002* paper IAEA-CN-94/TH/7-1 Ra

[49] L L Lao, H St John, R D Stambaugh, A G Kellman, W P Pfeiffer, Nucl. Fusion **25** (1985) 1611.

[50] S A Sabbagh, S M Kaye, J E Menard, *et al.*, Nucl. Fusion **41**, 1601 (2001).

[51] J D Strachan, B Grek, W Heidbrink, D Johnson, S M Kaye, H W Kugel, B LeBlanc, K McGuire, Nucl. Fusion **25** (1985) 863.

[52] D S Darrow, R Bell, D W Johnson, H Kugel, J R Wilson, R E Cecil, R Maingi, A Krasilnikov, A Alekseyev, Rev. Sci, Instrum. **72** (2001) 784.

[53] H.L. Berk, B.N. Breizman, J. Fitzpatrick, M.S. Pekker, H.V. Wong, and K.L. Wong, Phys. Plasmas **3**, 1827 (1996).

[54] C. Z. Cheng, Phys. Reports **211**, 1-51 (1992)

[55] D.Stutman M. Finkenthal, V. Soukhanovskii, M. J. May, H. W. Moos, and R. Kaita, Rev. Sci. Instruments **70** 572 (1999).

[56] S. Kaye, (manuscript in preparation).

[57] S. S. Medley and A. L. Roquemore, *Rev. Sci. Instrum.* **69**, 2651 (1998).

[58] S. S. Medley, R. E. Bell, M. P. Petrov, A. L. Roquemore and E. V. Suvorkin, Rev. Sci. Instrum., 74, March 2003, In Press.

[59] D S Darrow, S J Zweben, Z Chang, C Z Cheng, M D Diesso, E D Fredrickson, E Mazzucato, R Nazikian, C K Phillips, S Popovichev, M H Redi, R B White, J R Wilson, K L Wong, Nucl. Fusion **37** 939 (1997).

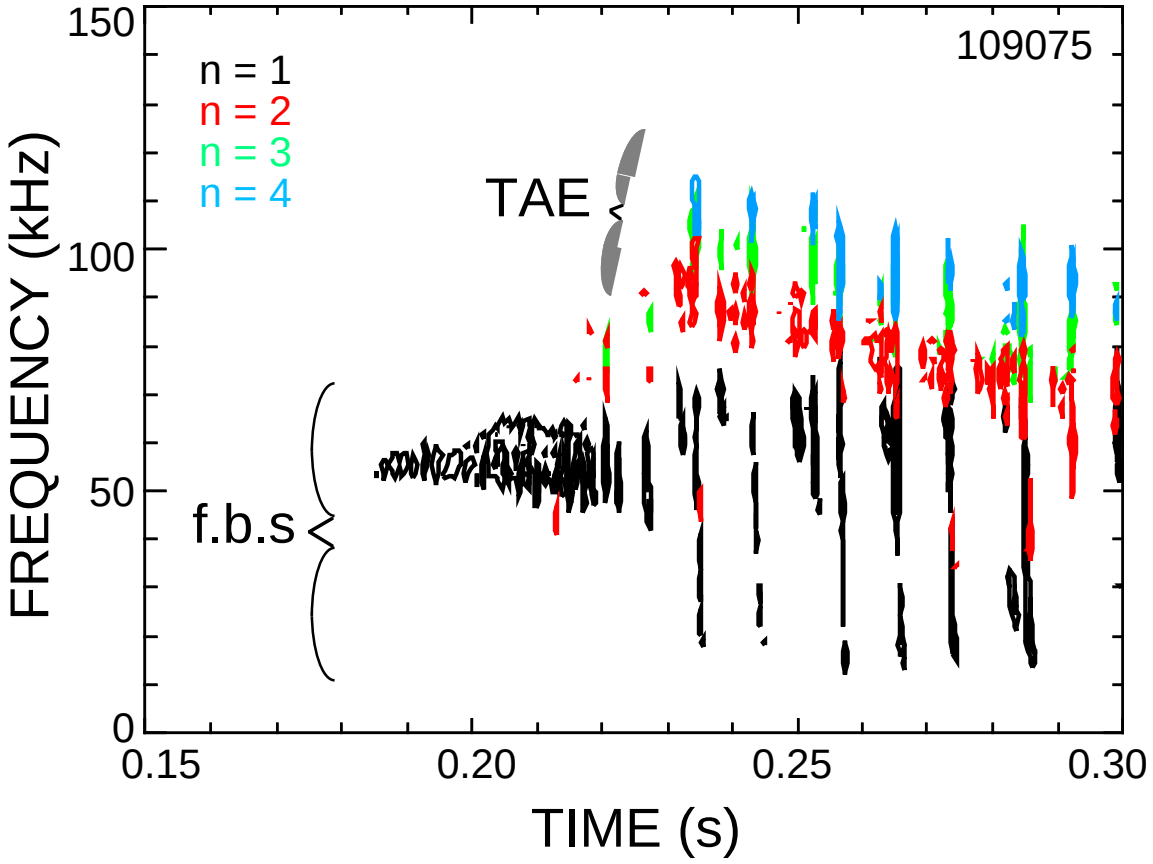

Figure 1. Spectrogram of the signal from a Mirnov coil on NSTX during neutral beam heating. Black contours indicate roughly n=1 modes, red n=2, green n=3, and blue n=4.

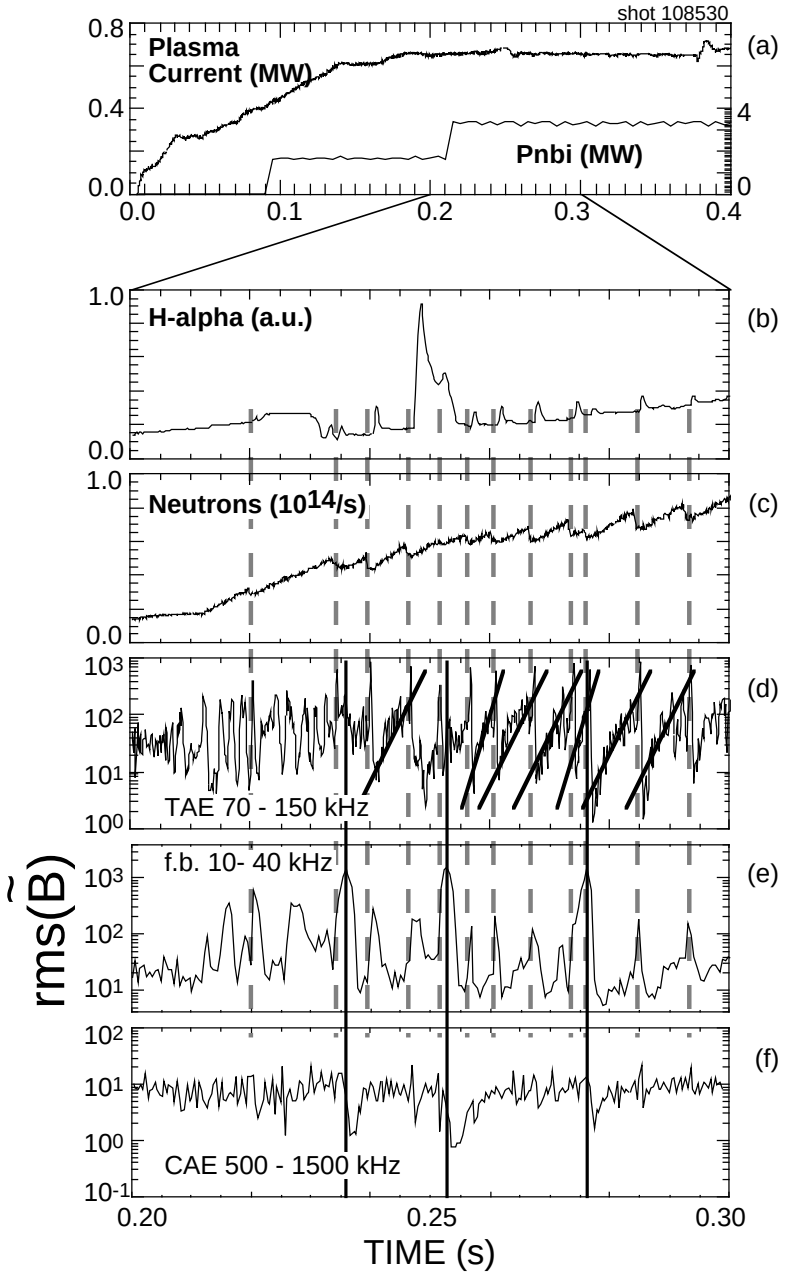

Figure 2. Typical evolution of an NSTX discharge. a) plasma current and neutral beam heating waveform, b) D-alpha light from the upper divertor plate, c) volume neutron emission, d) rms magnetic fluctuations in the 70 – 150 kHz band (TAE modes), e) rms magnetic fluctuation level in the frequency band 10 – 40 kHz (fishbones), f) rms magnetic fluctuation level in the 500 – 1500 kHz band (CAE modes).

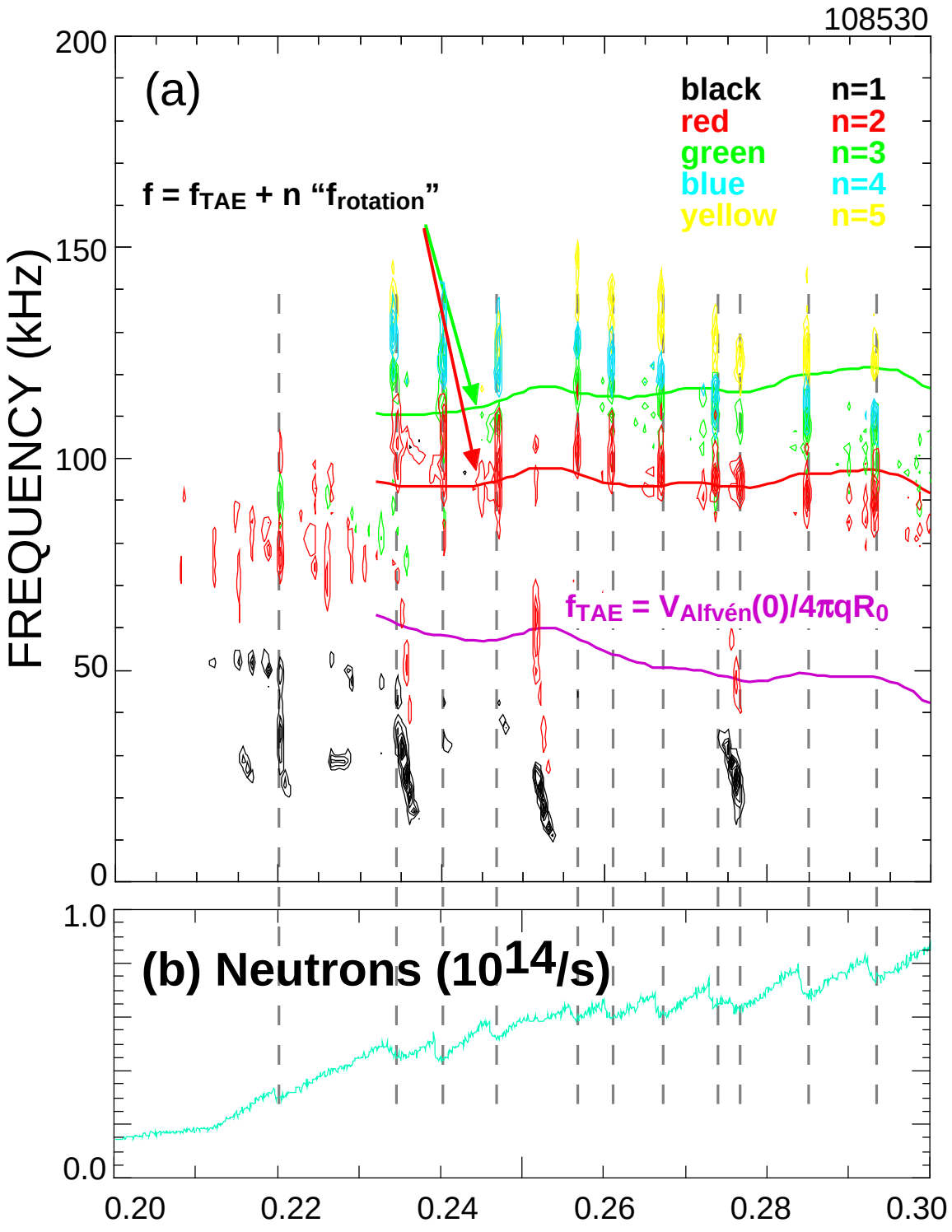

Figure 3. Spectrogram of magnetic fluctuations, (a), and neutron emissivity, (b), showing correlation of MHD bursts with neutron drops.

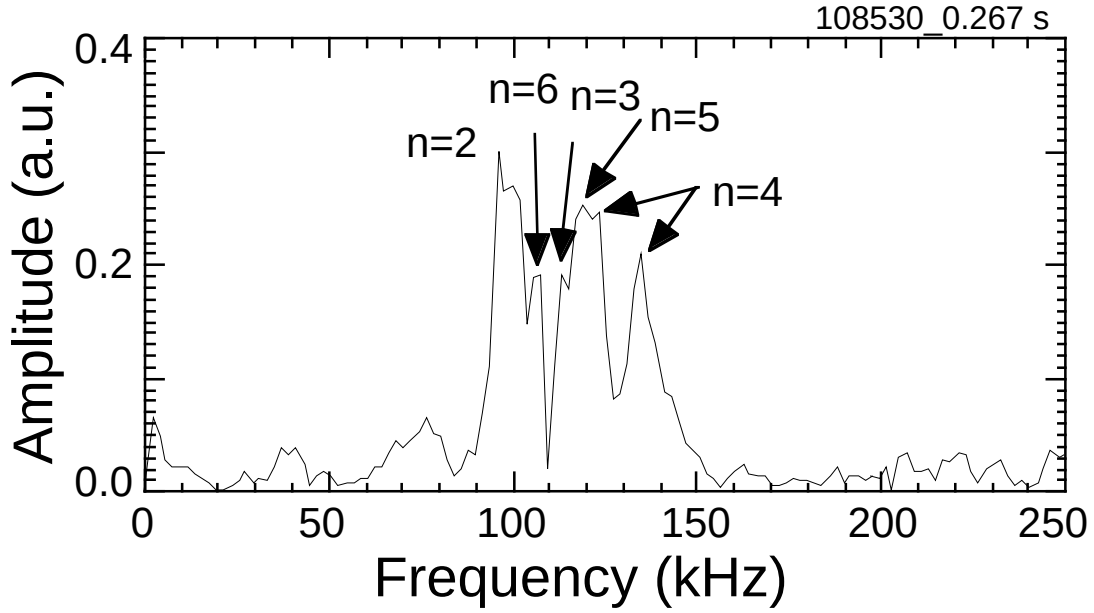

Figure 4. Spectrum of magnetic fluctuations with toroidal mode numbers indicated.

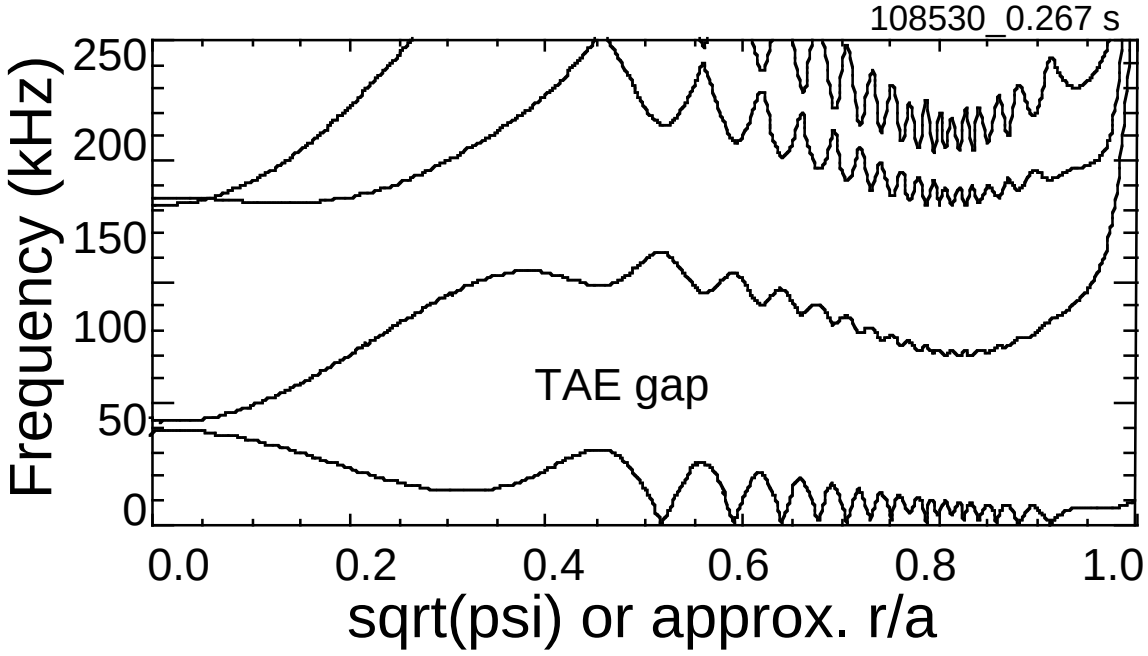

Figure 5. Gap structure calculated with NOVA-K for the n=2 modes.

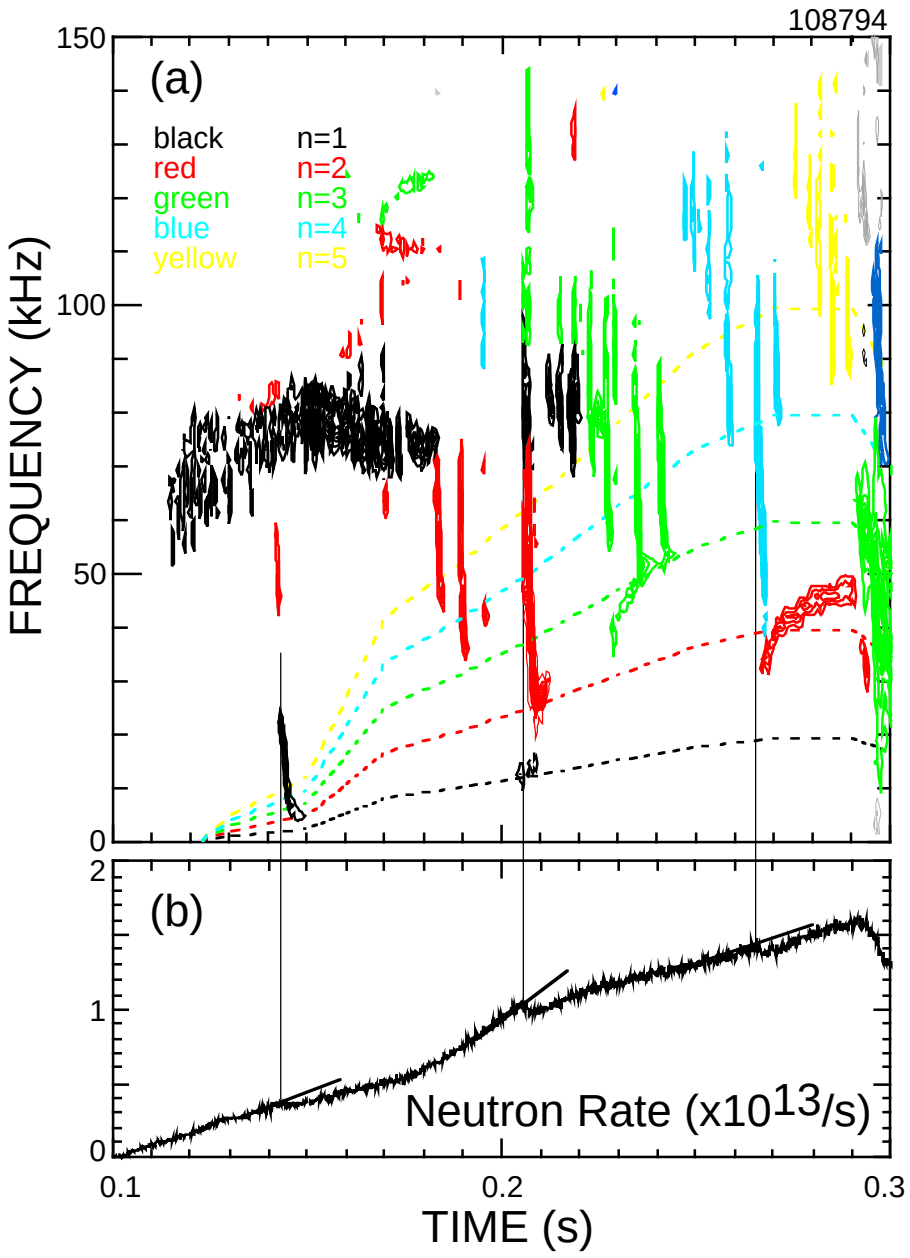

Figure 6. Mirnov coil spectrogram showing Type II and Type III fishbone activity, correlated with drops in the neutron emission (6b). (The mode numbers are indicated by color, black – n=1, red – n=2, green n=3, blue – n=4 and yellow – n=5.

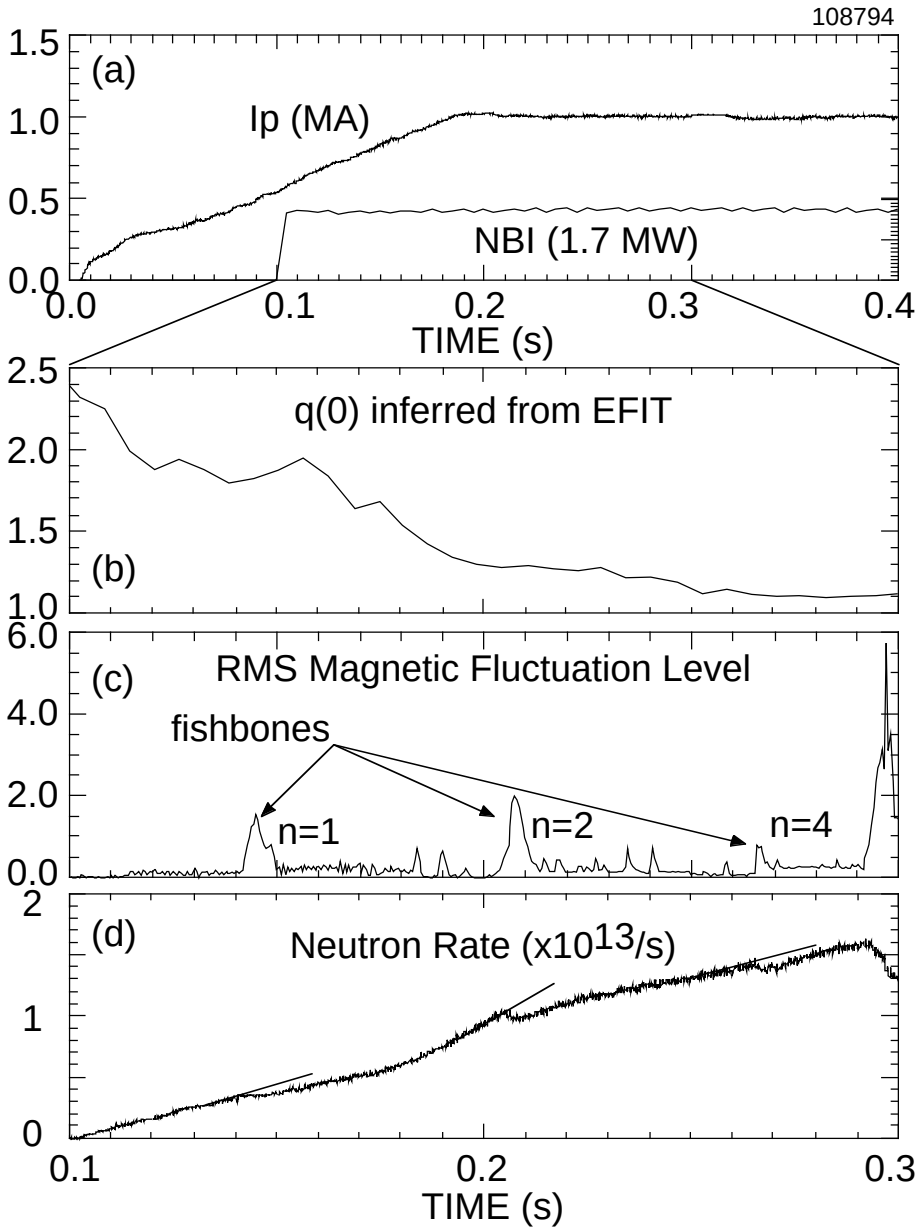

Figure 7. Waveforms showing the evolution of an NSTX discharge with fishbone activity. (a) plasma current and neutral beam heating power, (b) q(0) inferred from EFIT, (c) rms magnetic fluctuation level with the n=1, n=2 and n=4 fishbones correlated with neutron drops indicated, (d) neutron emission. (Fluctuation burst after 0.29 s is an MHD event, not fishbone.)

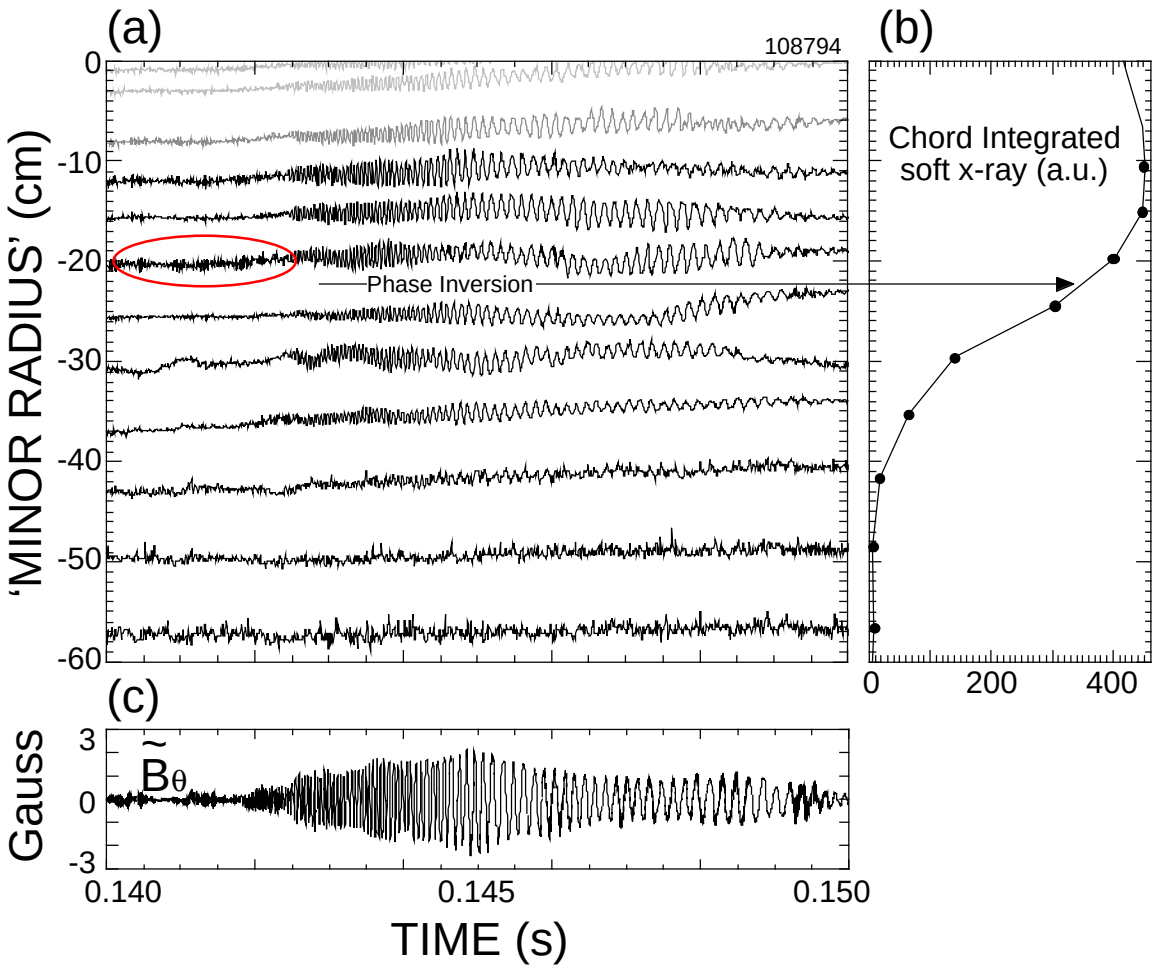

Figure 8a. Auto-scaled soft x-ray camera traces plotted at there approximate minor radius positions. Red circle indicates Type III fishbones.

Figure 8b. Chord integrated soft x-ray profile at 0.145s.

Figure 8c. Magnetic fluctuation level during this time period.

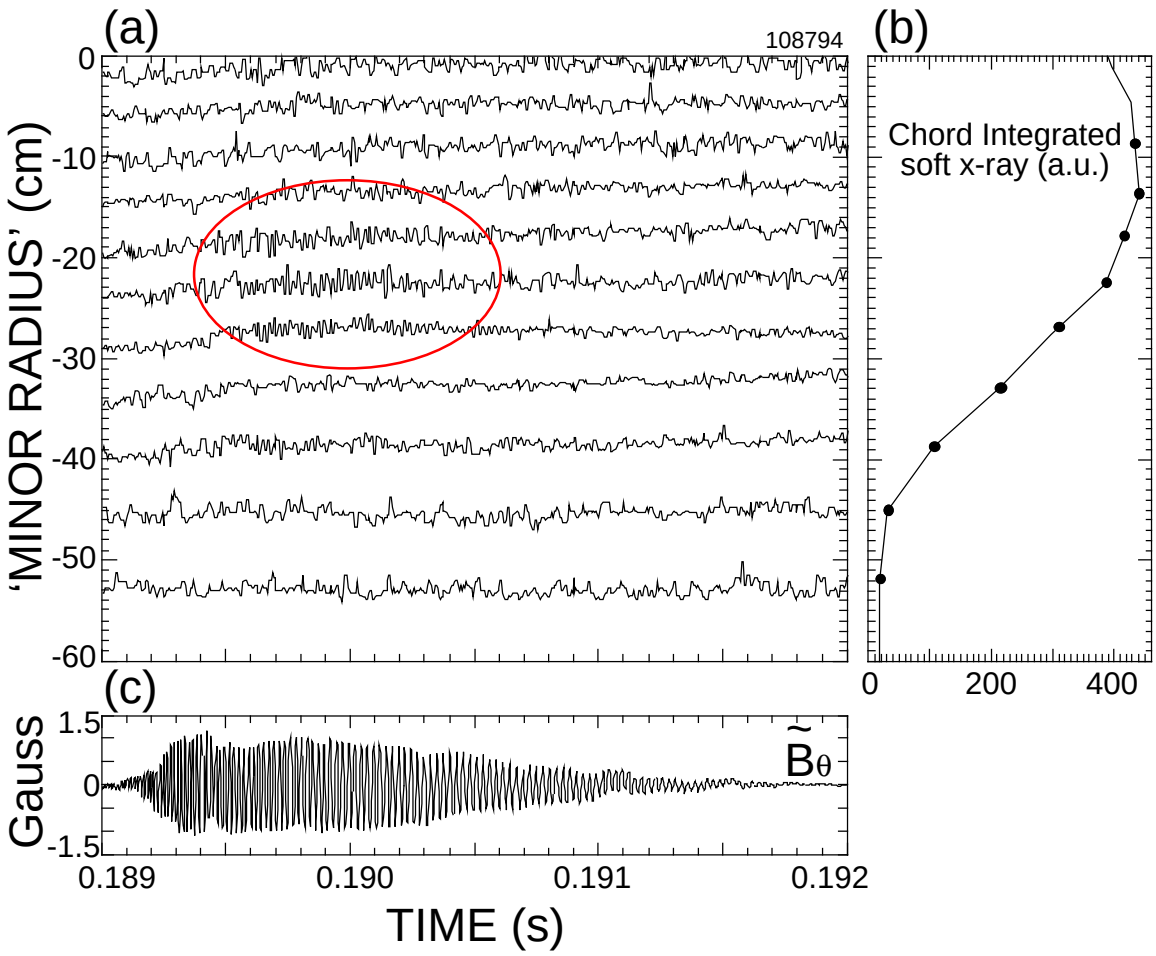

Figure 9a. Soft x-ray traces at their approximate radial locations showing a "weak" fishbone mode.

Figure 9b. Soft x-ray profile at 0.1905s.

Figure 9c. Integrated signal from Mirnov coil over this time interval.

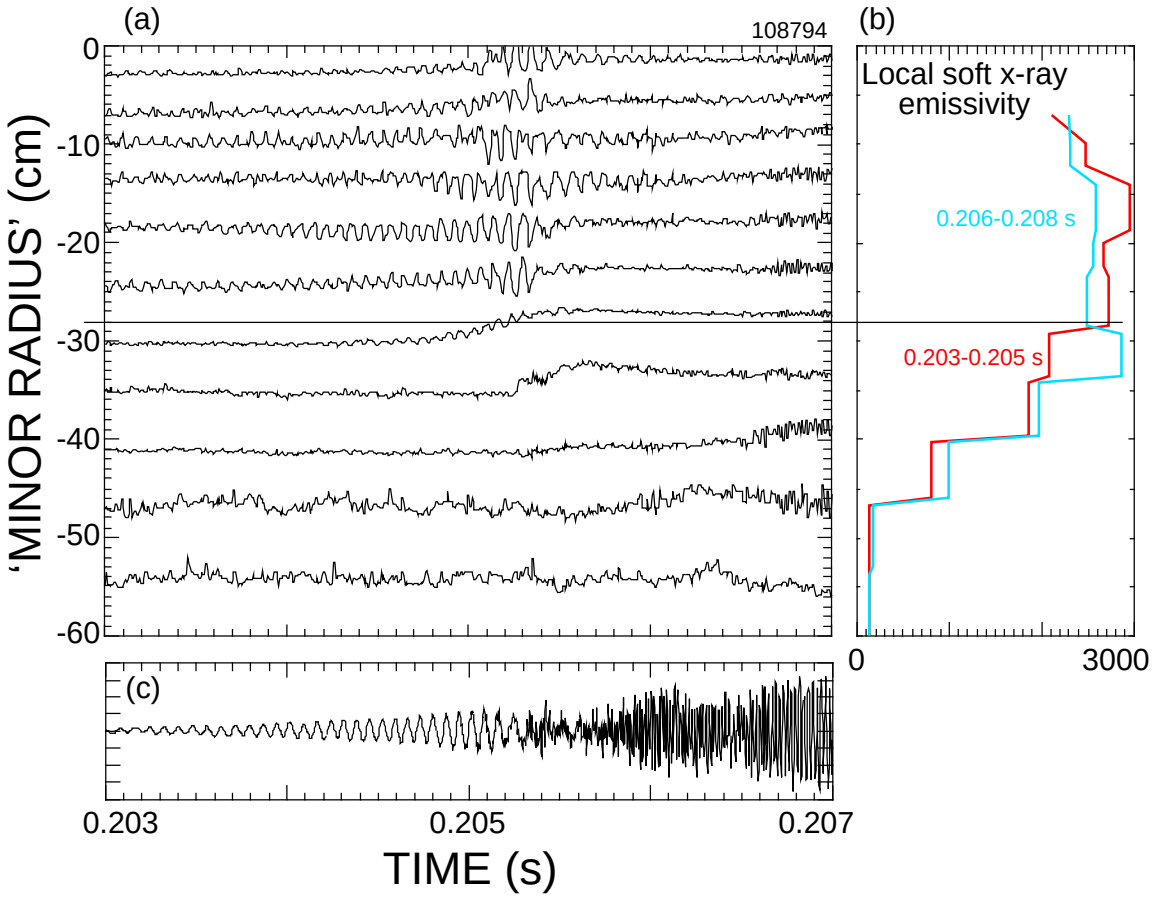

Figure 10a. Soft x-ray traces showing a sawtooth-like event, together with a low frequency precursor followed by a fishbone burst.

Figure 10b. Inverted soft x-ray profiles from before and after the 0.205 s showing the soft x-ray emissivity drops in the core and increases outside.

Figure 10c. Mirnov coil signal through this event.

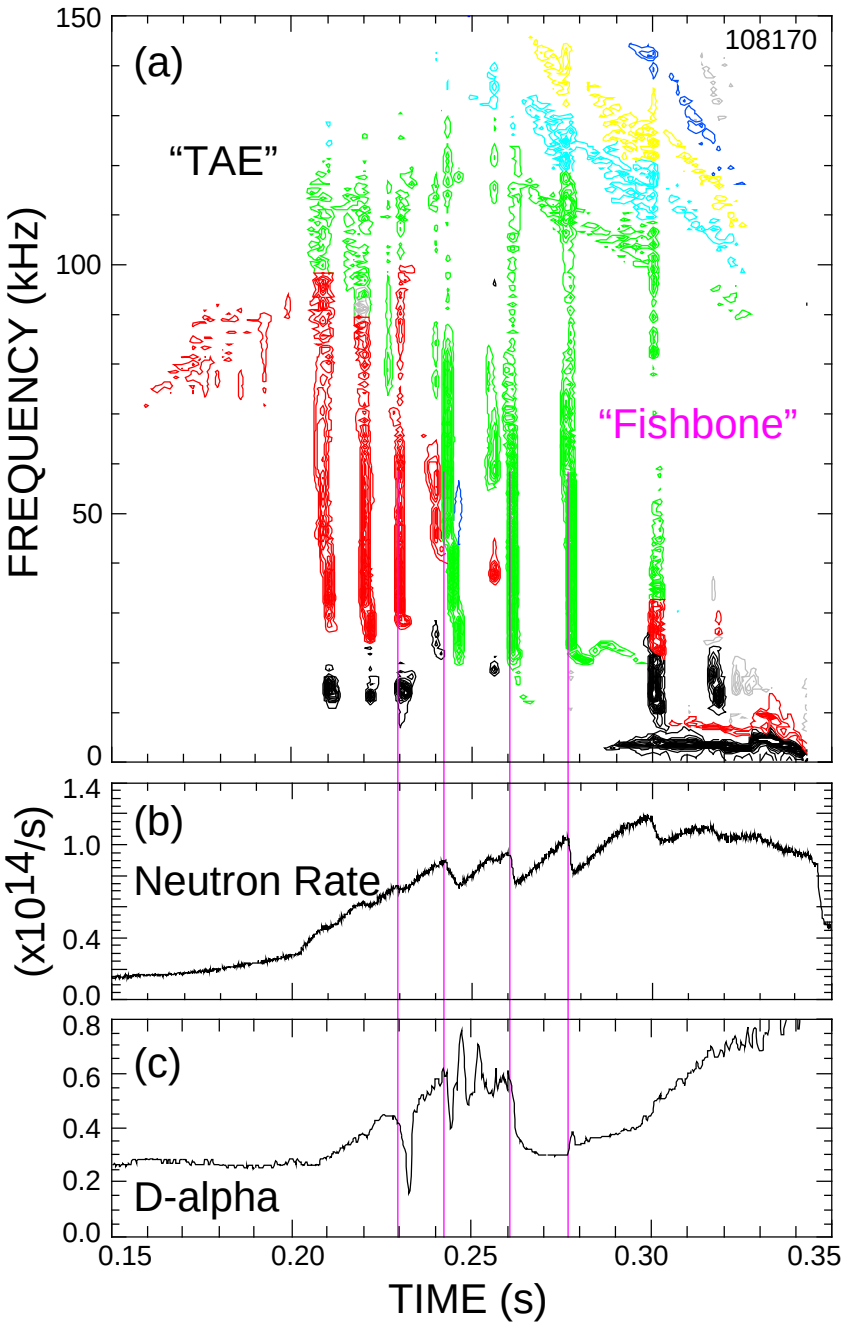

Figure 11a. Mirnov spectrogram showing fishbone bursts. Countour colors indicate inferred toroidal mode numbers; black – n=1, red – n=2, green – n=3, cyan – n=4, yellow – n=5 and blue – n=6.

Figure 11b. Neutron emissivity showing 20 % drops at fishbone bursts.

Figure 11c. D-alpha emsission drops for fishbones immediately prior to H-mode transition, small spike for fishbone after transition..

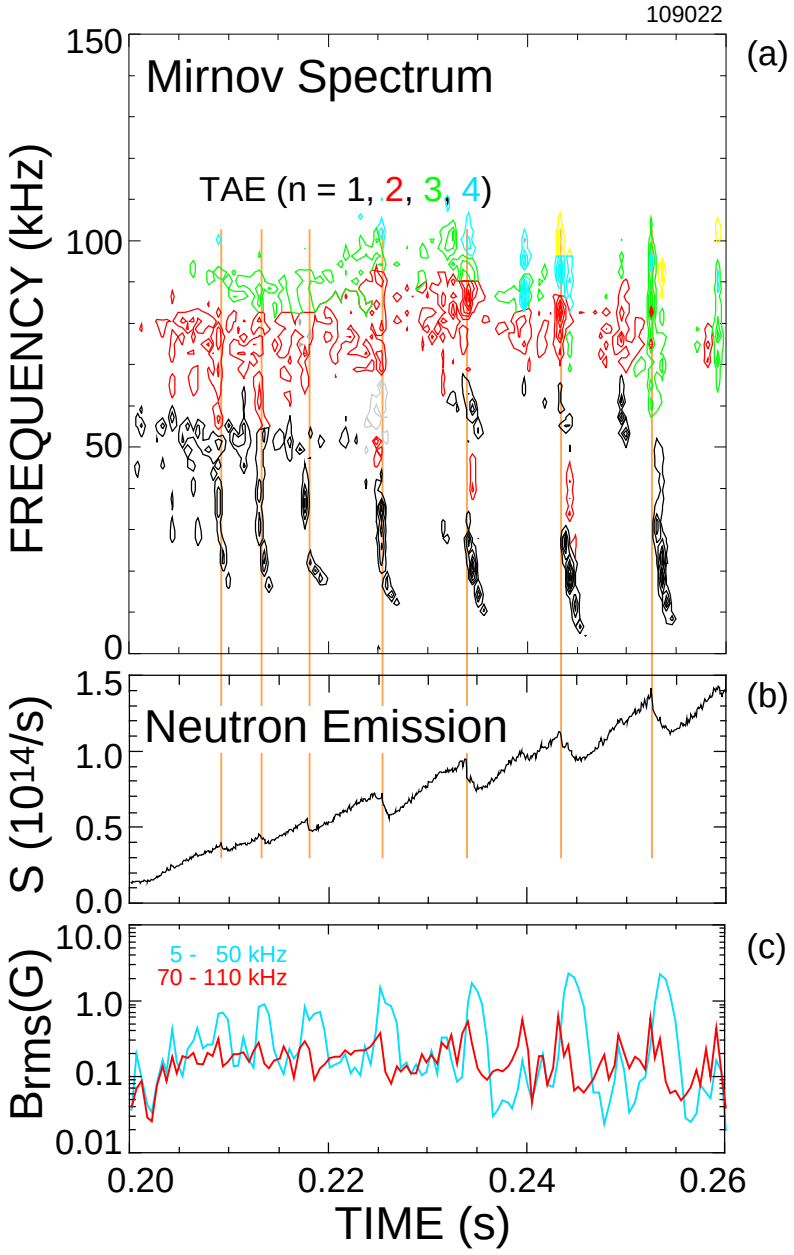

Figure 12a. Spectrogram of Mirnov coil showing combined fishbones and bursting TAE modes (black, red, green, blue, yellow correspond to n=1, 2, 3, 4, 5, respectively).

Figure 12b. Neutron emission showing up to 20 % drops at the combined MHD bursts.

Figure 12c. RMS magnetic fluctuation levels in the 5 – 10 kHz (blue) band and 70 – 110 kHz band (red) showing fishbone amplitude and TAE amplitude evolution, respectively.

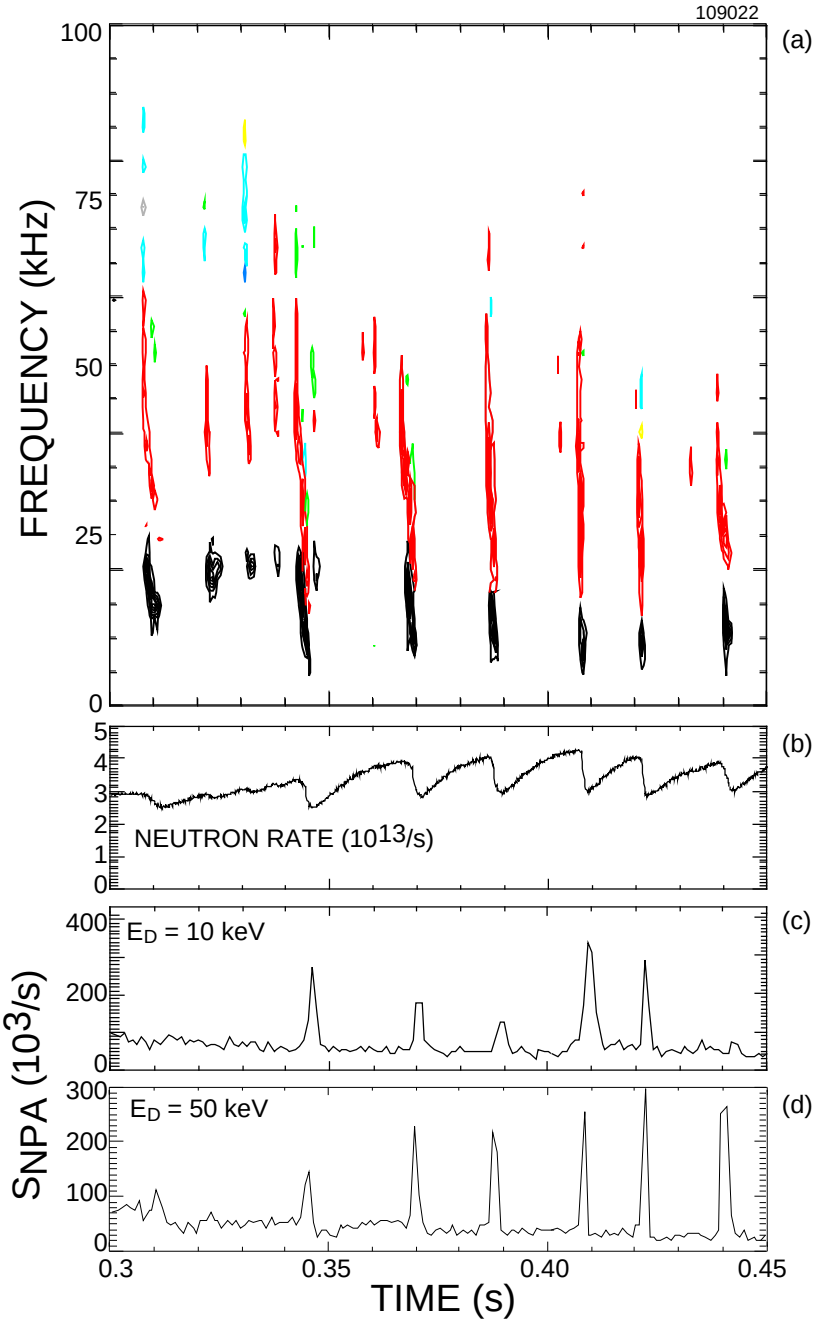

Figure 13a. Spectragram of Mirnov coil in latter half of discharge shown in Fig. 12.

Figure 13b. Neutron rate showing ≈ 25% drops in emissivity at each fishbone burst.

Figure 13c. Neutral particle analyzer signal showing 10 keVdeuterium channel.

Figure 13d. Neutral particle analyzer signal showing 50 keVdeuterium channel.

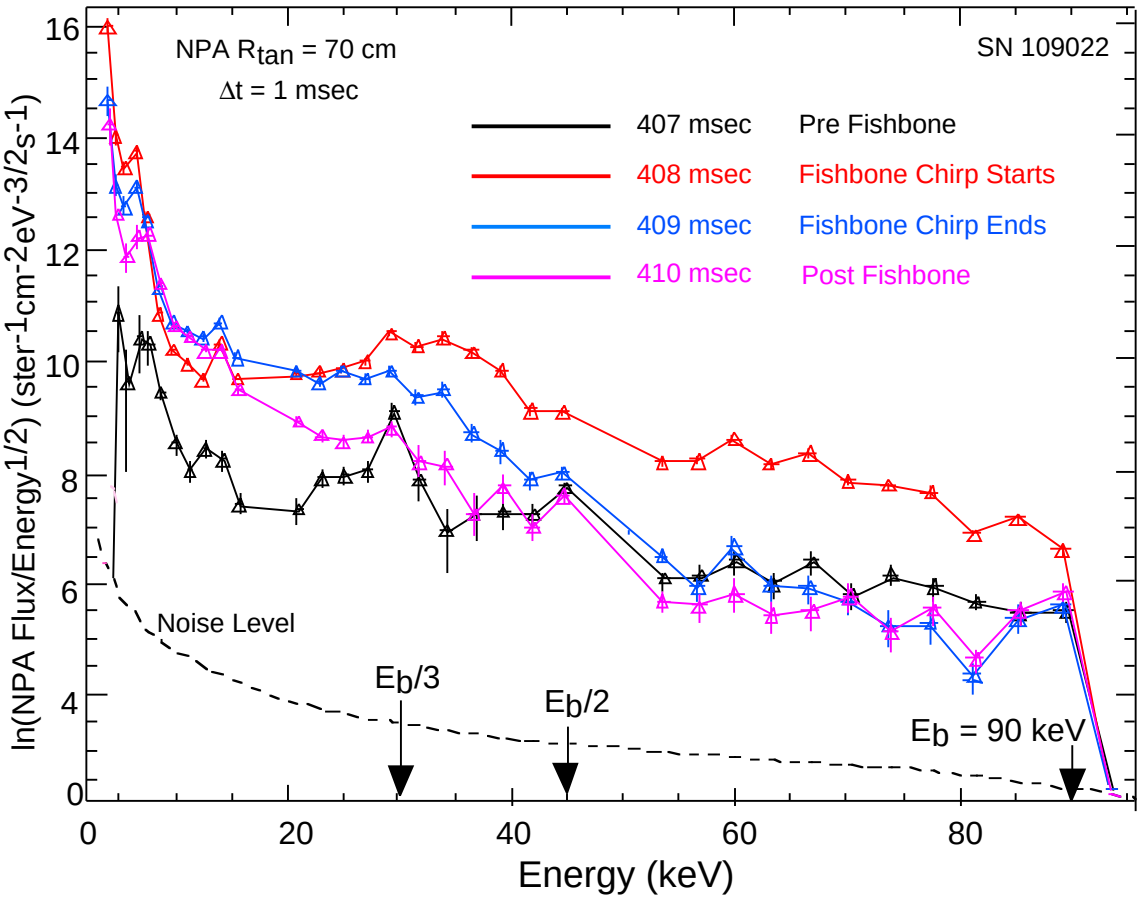

Figure 14. Fast ion spectra with full, half and third energy levels marked. Four time intervals are shown through a single fishbone event.

External Distribution

Plasma Research Laboratory, Australian National University, Australia
Professor I.R. Jones, Flinders University, Australia
Professor João Canalle, Instituto de Fisica DEQ/IF - UERJ, Brazil
Mr. Gerson O. Ludwig, Instituto Nacional de Pesquisas, Brazil
Dr. P.H. Sakanaka, Instituto Fisica, Brazil
The Librarian, Culham Laboratory, England
Mrs. S.A. Hutchinson, JET Library, England
Professor M.N. Bussac, Ecole Polytechnique, France
Librarian, Max-Planck-Institut für Plasmaphysik, Germany
Jolan Moldvai, Reports Library, MTA KFKI-ATKI, Hungary
Dr. P. Kaw, Institute for Plasma Research, India
Ms. P.J. Pathak, Librarian, Insitute for Plasma Research, India
Ms. Clelia De Palo, Associazione EURATOM-ENEA, Italy
Dr. G. Grosso, Instituto di Fisica del Plasma, Italy
Librarian, Naka Fusion Research Establishment, JAERI, Japan
Library, Plasma Physics Laboratory, Kyoto University, Japan
Research Information Center, National Institute for Fusion Science, Japan
Dr. O. Mitarai, Kyushu Tokai University, Japan
Library, Academia Sinica, Institute of Plasma Physics, People's Republic of China
Shih-Tung Tsai, Institute of Physics, Chinese Academy of Sciences, People's Republic of China
Dr. S. Mirnov, TRINITI, Troitsk, Russian Federation, Russia
Dr. V.S. Strelkov, Kurchatov Institute, Russian Federation, Russia
Professor Peter Lukac, Katedra Fyziky Plazmy MFF UK, Mlynska dolina F-2, Komenskeho Univerzita, SK-842 15 Bratislava, Slovakia
Dr. G.S. Lee, Korea Basic Science Institute, South Korea
Institute for Plasma Research, University of Maryland, USA
Librarian, Fusion Energy Division, Oak Ridge National Laboratory, USA
Librarian, Institute of Fusion Studies, University of Texas, USA
Librarian, Magnetic Fusion Program, Lawrence Livermore National Laboratory, USA
Library, General Atomics, USA
Plasma Physics Group, Fusion Energy Research Program, University of California at San Diego, USA
Plasma Physics Library, Columbia University, USA
Alkesh Punjabi, Center for Fusion Research and Training, Hampton University, USA
Dr. W.M. Stacey, Fusion Research Center, Georgia Institute of Technology, USA
Dr. John Willis, U.S. Department of Energy, Office of Fusion Energy Sciences, USA
Mr. Paul H. Wright, Indianapolis, Indiana, USA

The Princeton Plasma Physics Laboratory is operated
by Princeton University under contract
with the U.S. Department of Energy.

Information Services
Princeton Plasma Physics Laboratory
P.O. Box 451
Princeton, NJ 08543

Phone: 609-243-2750
Fax: 609-243-2751
e-mail: pppl_info@pppl.gov
Internet Address: http://www.pppl.gov